Published by IOP Publishing for Sissa Medialab

Received: *November 3, 2024*
Accepted: *December 20, 2024*
Published: *December 20, 2024*

Topical Workshop on Electronics for Particle Physics
University of Glasgow, Scotland, U.K.
30 September–4 October 2024

Radiation and magnetic field qualification of LVPS — a unified 12V DC power source for the CMS detector

K. Stachon[a,*] **G. Dissertori**[a] **T. Gadek**[a,b] **and W. Lustermann**[a] **on behalf of the CMS collaboration**

[a] *Institute for Particle Physics and Astrophysics, ETH Zurich, Otto-Stern-Weg 5, 8093 Zurich, Switzerland*
[b] *Advanced Power Semiconductor Laboratory, Physikstrasse 3, 8092 Zurich, Switzerland*

E-mail: krzysztof.stachon@proton.me

Abstract: Efforts aiming at consolidating the powering for the CMS detector have led to the development of a Low Voltage Power Supply (LVPS). The LVPS converts 380 V DC to 12 V DC, suitable for powering the widely used bPOL12V point-of-load DC-DC converter. To limit cable size, the LVPS must be hosted in the CMS experimental cavern, being exposed to ionizing radiation and stray magnetic field of up to 120 mT. The device is made of Commercial Off-The-Shelf (COTS) components, therefore, thorough qualifications at various design stages were performed to ensure its reliable operation in the harsh environmental conditions for the HL-LHC era.

Keywords: Voltage distributions; Modular electronics; Radiation-hard electronics

*Corresponding author.

https://doi.org/10.1088/1748-0221/19/12/C12016

1 Introduction

The CMS Phase-2 Upgrade [1, 2] on-detector electronics require operational voltage levels ranging typically from 1.2 V to 2.5 V DC. Electrical power is delivered from the power grid to the Point-of-Load (POL) via three intermediate voltage conversion stages. The first stage converts three-phase 230 V AC into 380 V DC using a Commercial off-the-shelf (COTS) AC-DC power conversion system [3]. The second stage uses Low Voltage Power Supply (LVPS) to step-down from 380 V DC to 12 V DC, the input voltage required by the POL converters. The LVPS are located in the CMS experimental cavern approximately 30 m away from the on-detector electronics in a moderately harsh radiation and magnetic field environment. The third stage employs CERN's radiation tolerant bPOL12V [4, 5] and linPOL12V converter ASICs, embedded into the on-detector electronics.

1.1 LVPS — Low Voltage Power Supply

The LVPS must operate in the radiation and magnetic field of the CMS experimental cavern with a required tolerance of up to 32 Gy Total Ionizing Dose (TID), 2×10^{11} HEH cm^{-2} (>20 MeV) High Energy Hadron Fluence (HEH), and 1×10^{13} n cm^{-2} (1 MeV equivalent) neutron fluence. This will cover expected radiation levels during the HL-LHC era with margin, corresponding to integrated luminosity of 4000 fb^{-1}. Furthermore, the device must remain operational in the presence of an external static magnetic field of up to 120 mT.

The development and production of the LVPS have been outsourced by CERN to industry. Nonetheless, we implemented rigorous monitoring to ensure compliance with specifications. In addition, we conducted radiation and magnetic-field evaluations on prototypes. The outcomes of these evaluations are presented in this manuscript.

The LVPS feature an input voltage ranging from 342 V to 400 V DC and output voltages ranging from 7 V to 13 V DC. The LVPS building block is a 720 W module with up to ten of them fitting a 5U tall 19 ” chassis, featuring water cooling. A modular design, allows for 3 different module configurations: 12 channels of 60 W, 6 channels of 120 W, or 3 channels of 240 W. Each module in the chassis is individually remote controlled using CAN-BUS. All module outputs are individually protected by dedicated, redundant over-voltage protection, ensuring output voltages are staying below an adjustable threshold. This additional protection was introduced to protect bPOL12V against voltage transients.

Three CMS sub-detectors joined in a common procurement project requiring about 1000 modules, corresponding to 720 kW total output power.

2 Radiation qualification

2.1 Qualification strategy

The LVPS is designed using COTS components. While this methodology significantly reduces cost, it requires thorough radiation testing during the development phase, as electronic components typically deviate from their specified performance parameters when irradiated. The damage is caused by several effects of ionising radiation, such as Total Ionizing Dose (TID), displacement damage and Single Event Effect (SEE). The latter two can originate as well from hadron-induced damage. SEEs are special as a single interaction can potentially damage an electronic components or induce errors within digital electronics. In power electronics components, the most critical effect is Single Event Burnout (SEB), caused by radiation-induced breakdowns in power transistors [6].

2024 JINST 19 C12016

The LVPS development started with component selection for gate drivers, Analog-to-Digital Converters (ADCs), and Digital-to-Analog Converters (DACs), using CERN's radiation working group [7] database, and component-level radiation screening tests at Paul Scherrer Institute (PSI)'s Proton Irradiation Facility (PIF). Subsequently, system-level tests were conducted at the CERN's CHARM mixed-field irradiation facility, providing conditions as found in the experiments. These tests were meticulously prepared and executed by us, while the Device Under Tests (DUTs) have been supplied by the development contractor: Kontron HARTMANN-WIENER.

2.2 Results

Since 2021, five irradiation campaigns have been completed. The result of the three most recent ones, including testing of full prototypes: Prototype-I and Prototype-II, are reported below.

2.2.1 June 2023 test at CHARM

The goal of this test was the evaluation of the Over-Current Protection (OCP) circuit, and of the micro-controller including Controller Area Network (CAN) communication.

The microcontroller was tested by sending a series of queries every second. The communication was stable throughout the test, except one case, where a query missed the response. This was not considered a problem, because all subsequent queries were answered correctly.

The OCP circuit comprises a current measurement shunt resistor (100 mΩ), followed by a differential amplifier, and a latching comparator with threshold and RESET inputs, and over-current protection signal (V_{OCP}) output (figure 1). It was evaluated by controlling the voltage across the shunt resistor, creating a cyclic current test pattern (figure 2) of 60 s duration. The current first crosses the threshold trigger the comparator, then it is lowered just below the threshold, the comparator is reset, and V_{OCP} is monitored checking for spurious triggers. Two test boards with two sets of components have been tested: set A hosting amplifier: Onsemi LM358D, comparator: Onsemi LM293M, and set B hosting amplifier and comparator: MC34072.

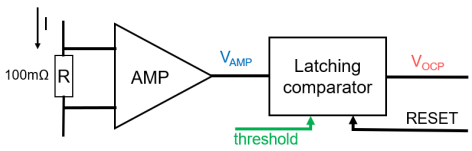

Figure 1. Schematic view of OCP circuit.

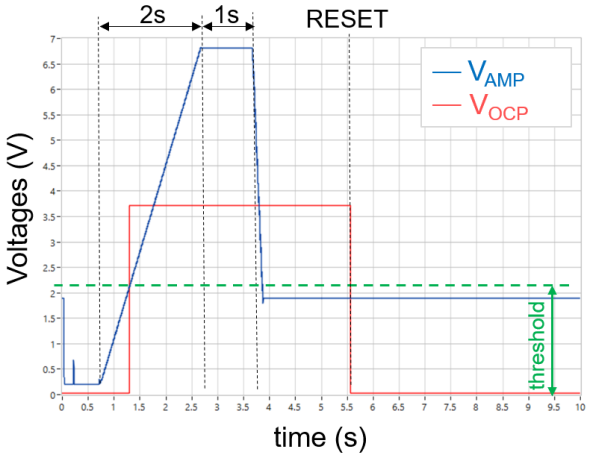

Figure 2. One cycle of the OCP test pattern with typical amplifier and latching comparator outputs.

Previous tests revealed the presence of radiation-induced spurious OCP tripping. In this test, all comparators output voltages were sampled with 600 kS/s enabling waveform reconstruction. This revealed that spikes are permanently present and have a typical waveform (figure 3) that may be filtered out. Moreover, a small drifts of the comparator thresholds was measured (figure 4), with test set A performing, slightly better showing a total drift of 1.3 % at 32 Gy TID.

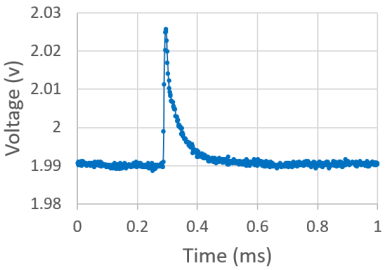

Figure 3. Typical radiation-induced spike.

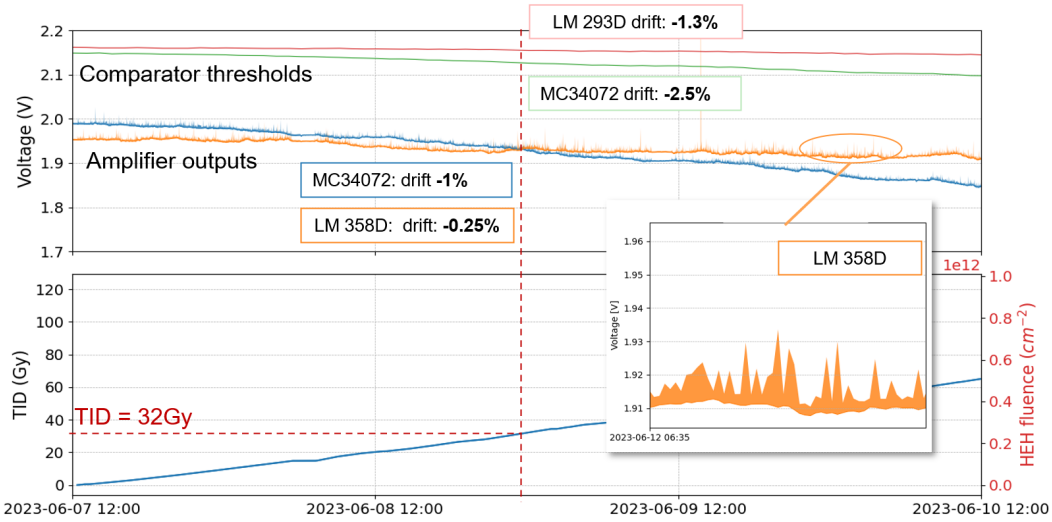

Figure 4. OCP circuit amplifier and compactor drifts versus TID at constant input current.

2.2.2 October 2023 test at CHARM

Prototype-I, was evaluated at CERN Highly-Accelerated Mixed Field Facility (CHARM) for two weeks. The setup comprised a chassis and three modules, one per configuration, 12, 6, and 3-channel. During the test all input and output voltages and currents of all 21 channels were continuously monitored at 50% of full load, and every three hours a test sequence was executed, including input power cycling, idle current mesurement, OCP test, efficiency measurements and more. All output voltage remained stable (figure 5), with minor radiation-induced few mV jumps. Figure 6 shows the exceptional occurrence of a 25 mV jump.

All three modules failed to boot at TIDs between 30 Gy and 47 Gy. The root cause was traced to the LM317 linear regulator, which had been sourced from a different manufacturer than specified. Moreover, CAN communication was intermittently lost, although rebooting resolved the issue. One channel failed at a TID of 100 Gy, 3-times higher than required.

2024 JINST 19 C12016

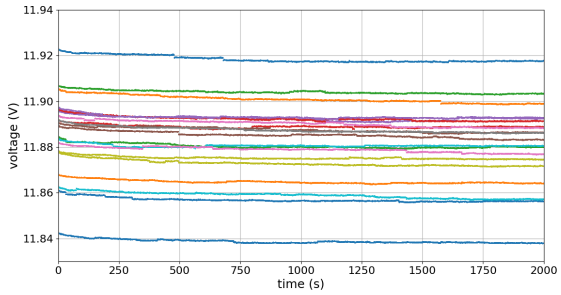

Figure 5. Typical voltage waveform for 21 channels tested. Acquired at 30 Gy.

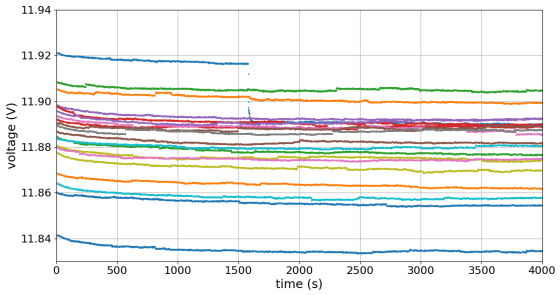

Figure 6. Voltage jump registered at 35 Gy in one channel (blue) out of 21 tested.

2.2.3 June 2024 test at CHARM

Prototype-II was tested at CHARM for two weeks. Issues identified in Prototype-I had been resolved. However, a new problem was discovered. The output current measurement is drifting significantly as a function of TID, resulting in 20 % to 40 % deviation from the trues. See figure 7 for a typical channel. This compromises the OCP feature.

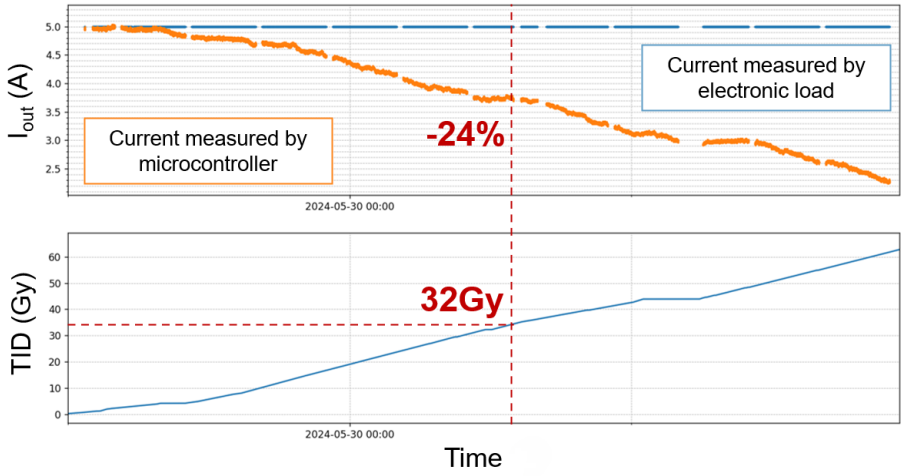

Figure 7. Drift of output current measurement (orange) with 5 A constant load (blue), typical channel.

Additionally, SEEs caused failures of the ADuM3152ARSZ digital isolators, rendering the concerned channel not controllable. One such failure had been observed in the previous test while this time 5 out of 21 channels were affected. However, the channels were exposed to over 5 times higher HEH fluence than the lifetime exposure. We estimate the upper limit cross-section $\hat{\sigma}$ for this failure with 95% confidence level following reference [8]: $\hat{\sigma} = \frac{\chi^2_{2(d+1),0.95}}{2\sum_{i=1}^{N}\Phi_i} \approx 3.29 \times 10^{-14}\,\mathrm{cm}^2$, with N being the number of devices, d the number of observed failures, and Φ_i the fluence received by device i, i = 1 . . . N. Although the cross-section is relatively low, it was decided to mitigate the problem by replacing the component with a combination of other digital isolators: ADUM3401BRWZ and ADUM3402BRWZ.

2024 JINST 19 C12016

3 Magnetic field qualification

In November 2023 Prototype-I was tested in a magnet. We measured efficiency as function of the external magnetic field in a range from 0 mT to 153 mT in three orthogonal orientations. The expected minimum LVPS efficiency for loads >40% of full load is 88%. Satisfactory performance was observed solely in one orientation (figure 8), whereas the other orientations (figures 9, 10) exhibited considerable efficiency degradation attributable to the magnetic field. Subsequent investigations identified a transformer fitted with a magnetic shield as the root cause. The shield, manufactured from high-purity iron, had not been subjected to thermal annealing post-machining. Computational simulations using COMSOL indicated that thermal annealing significantly enhances the performance of the shield, sufficient to cure the observed problem.

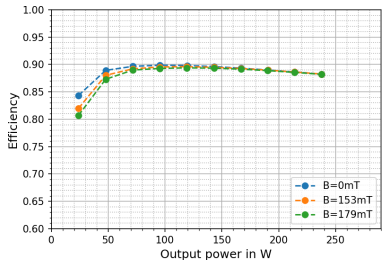

Figure 8. X orientation.

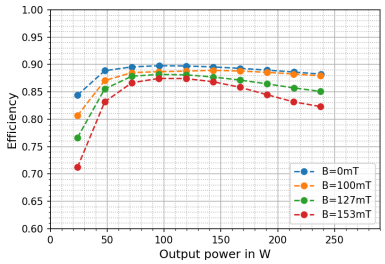

Figure 9. Y orientation.

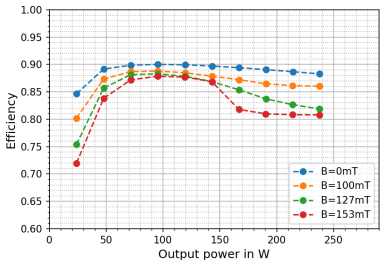

Figure 10. Z orientation.

4 Summary and conclusions

Comprehensive radiation and magnetic field qualification of newly developed LVPSs were performed on both components and full prototypes. The tests demonstrated the viability of the LVPSs prototypes for the CMS detector under HL-LHC conditions in the specified, harsh radiation and magnetic field environment.

Key findings of the radiation tests are: the LVPSs voltage regulation is stable, with minor, non-critical radiation-induced voltage jumps. There are radiation-induced spikes in the OCP circuitry, but due to its consistent shape, these will be filtered out. Dose-related boot failures and occasional CAN communication losses were observed. They were either mitigated or occurred beyond the specified TID. The use of COTS components posed severe challenges, particularly in maintaining the robustness of regulators such as the LM317, highlighting the importance of strict component sourcing and thorough qualification.

Magnetic field tests revealed orientation-dependent efficiency degradation. Electromagnetic simulations suggested that thermal annealing of the magnetic shield would alleviate these inefficiencies and extend the operational performance of the LVPS. Consequently, the magnetic shield of all future LVPS, prototypes, and production, will be thermally annealed.

Overall, the LVPS has demonstrated strong potential, and with the identified issues addressed in future iterations, it is well on its way to meeting the operational requirements of CMS at the HL-LHC. The next and likely final iteration will feature improved current measurement accuracy and specified performance in all magnetic field orientations.

2024 JINST 19 C12016

Acknowledgments

The authors thank Michael Dröge and Christian Haller from ETH Zurich for their invaluable support in preparing and installing the tests setups, and the Kontron HARTMANN- WIENER engineers, for providing the DUTs, and their contributions to the preparation of the June 2024 radiation test.

This work was supported by the Swiss National Science Foundation, SNF FLARE 201476 grant.

References

[1] CMS collaboration, *The CMS Experiment at the CERN LHC*, 2008 *JINST* **3** S08004.

[2] CMS collaboration, *Development of the CMS detector for the CERN LHC Run 3*, 2024 *JINST* **19** P05064 [arXiv:2309.05466].

[3] K. Stachon et al., *Modern high-availability multi-stage power distribution system for the CMS phase-2 upgrade*, 2023 *JINST* **18** C02053.

[4] F. Faccio et al., *The bPOL12V DCDC converter for HL-LHC trackers: towards production readiness*, *PoS* **370** (2020) 070.

[5] bPOL12V v6 datasheet v1.5, accessible as of October 2024, https://power-distribution.web.cern.ch/assets/datasheets/bPOL12V_V6datasheetV1.9.pdf.

[6] A. Holmes-Siedle and L. Adams, *Handbook of Radiation Effects. Second edition*, Oxford University Press (2002) [DOI:10.1093/oso/9780198507338.001.0001].

[7] CERN RadWG components database, https://radwg.web.cern.ch/.

[8] Texas Instruments, *Application note: Single-Event Effects Confidence Interval Calculations*, https://www.ti.com/lit/pdf/slvk047 (2020).

2024 JINST 19 C12016